The Cryosphere Discuss., https://doi.org/10.5194/tc-2018-155
Manuscript under review for journal The Cryosphere
Discussion started: 1 August 2018

Brief communication: Pancake ice floe size distribution during the winter expansion of the Antarctic marginal ice zone

Alberto Alberello[1,*], Miguel Onorato[2,3], Luke Bennetts[4], Marcello Vichi[5,6], Clare Eayrs[7], Keith MacHutchon[8], and Alessandro Toffoli[1]

[1]Department of Infrastructure Engineering, The University of Melbourne, Parkville, VIC 3010, Australia.
[2]Dipartimento di Fisica, Università di Torino, Torino, 10125, Italy.
[3]INFN, Sezione di Torino, Torino, 10125, Italy.
[4]School of Mathematical Sciences, University of Adelaide, Adelaide, SA 5005, Australia
[5]Department of Oceanography, University of Cape Town, Rondenbosch, 7701, South Africa.
[6]Marine Research Institute, University of Cape Town, Rondenbosch, 7701, South Africa.
[7]Center for Global Sea Level Change, New York University Abu Dhabi, Abu Dhabi, United Arab Emirates.
[8]Department of Civil Engineering, University of Cape Town, Rondenbosch, 7701, South Africa.
[*]now at: School of Mathematical Sciences, University of Adelaide, Adelaide, SA 5005, Australia

Correspondence: Alberto Alberello (alberto.alberello@outlook.com)

Abstract.

The size distribution of pancake ice floes is calculated from images acquired during a voyage to the Antarctic marginal ice zone in the winter expansion season. Results show that 50 % of the sea ice area is made up by floes with diameters 2.3–4 m. The floe size distribution shows two distinct slopes on either side of the 2.3–4 m range. It is conjectured that growth of pancakes from frazil forms the distribution of small floes ($D < 2.3$ m), and welding of pancakes forms the distribution of large floes ($D > 4$ m).

1 Introduction

Prognostic floe size distributions are being integrated into the next generation of large-scale sea ice models (Horvat and Tziperman, 2017; Bennetts et al., 2017; Roach et al., 2018a). Early results show that the floe size distribution has the greatest impacts on ice concentration and volume close to the ice edge, in the marginal ice zone, where ocean waves regulate floe sizes and floes are generally the smallest, meaning they are prone to melting in warmer seasons. However, at present the only field data available to validate and improve the models are empirical distributions derived for pack ice formed from ice breakup due to winds, waves and currents, and spanning several orders of magnitude (from few meters to tens of kilometres; e.g. Toyota et al., 2016).

Break up of pack ice often exhibits a fractal behaviour similarly to many brittle materials (Gherardi and Lagomarsino, 2015). It has been argued that exceedance probability of the characteristic floe size D expressed as number of floes follows a power law $N(D) \propto D^{-\alpha}$, where the scaling exponent $\alpha = 2$ if a fractal behaviour is assumed (Rothrock and Thorndike, 1984). Observations, from both the Arctic and Antarctic, do not support the existence of a unique scaling exponent (Steer et al., 2008; Toyota et al., 2011), with two distinct scaling exponents of the exceedance probability reported. For small floes (tens of metres and below) the exponent is $\alpha = 1.03$–1.52, while for larger floes $\alpha = 3.40$–7.59 (Toyota et al., 2011).

The validity of power law scaling has not been demonstrated yet and its adoption is mostly justified by the wide range of floes diameters (Horvat and Tziperman, 2017; Stern et al., 2018). Scaling parameters are typically estimated on the log-log plane with a least square fit, and, as noted by Stern et al. (2018), without rigorous goodness-of-fit tests. In comparison, Herman et al. (2017) examined the size distribution of floes under the action of waves in controlled laboratory experiments, by analysing the probability density function $n(D)$, which revealed a fractal response due to an arbitrary strain (a power law) superimposed to a Gaussian break up process induced by the waves. The interplay of these mechanisms is hidden in the floe number exceedance probability.

Existing observations do not provide quantitative descriptions of the floe size distribution for pancake ice floes, which form from frazil ice under the continuous action of waves and thermodynamic freezing processes (Shen et al., 2004; Roach et al., 2018b). This is important, for example, during the Antarctic winter sea ice expansion, when hundreds of kilometres of ice cover around the Antarctic continent is composed of pancake floes of roughly circular shape and characteristic diameters 0.3–3 m (Worby et al., 2008). Pancake floes represent most of the sea ice annual mass budget (Wadhams et al., 2018). Moreover, in the Arctic, pancakes are becoming more common due to the increased wave intensity associated with the ice retreat (Roach et al., 2018b).

Shen and Ackley (1991) reported pancake floe sizes from aerial observations collected during the Winter Weddell Sea Project (July 1986), showing that pancake sizes increase with distance from the ice edge, from 0.1 m in the first 50 km up to ≈ 1 m within 150 km from the edge. They attributed this to the dissipation of wave energy with distance into the ice-covered ocean, and proposed a relationship between wave characteristics, mechanical ice properties and pancake size (Shen et al., 2004). More recently, Roach et al. (2018b) used camera images acquired from SWIFT buoys deployed in the Beaufort Sea (Sea State cruise, October–November 2015) to quantify the lateral growth of pancakes and their welding. The high correlation between wave properties and the size of relatively small pancakes (up to 0.35 m) was confirmed.

To our knowledge, the pancake floe size distribution has yet to be characterised. Here, a new set of images from the Antarctic marginal ice zone are used to measure the shape of individual pancakes and to infer their size distribution.

2 Sea ice image acquisition

At approximately 07:00 UTC on the 4th of July 2017, the icebreaker S.A. Agulhas II entered the marginal ice zone between 61° and 63° South and approximately 30° East during an intense storm (see Fig. 1a,b for the ship track and a snapshot of peak wave period and significant wave height as sourced from ECMWF ERA-Interim reanalysis, Dee et al. 2011). A buoy was deployed in the marginal ice zone ≈ 100 km from the ice edge (green mark in Fig. 1c). At the time of deployment, the significant wave height was 5.5 m, with maximum individual wave height of 12.3 m. The dominant wave period was 15 s.

The Cryosphere Discuss., https://doi.org/10.5194/tc-2018-155
Manuscript under review for journal The Cryosphere
Discussion started: 1 August 2018

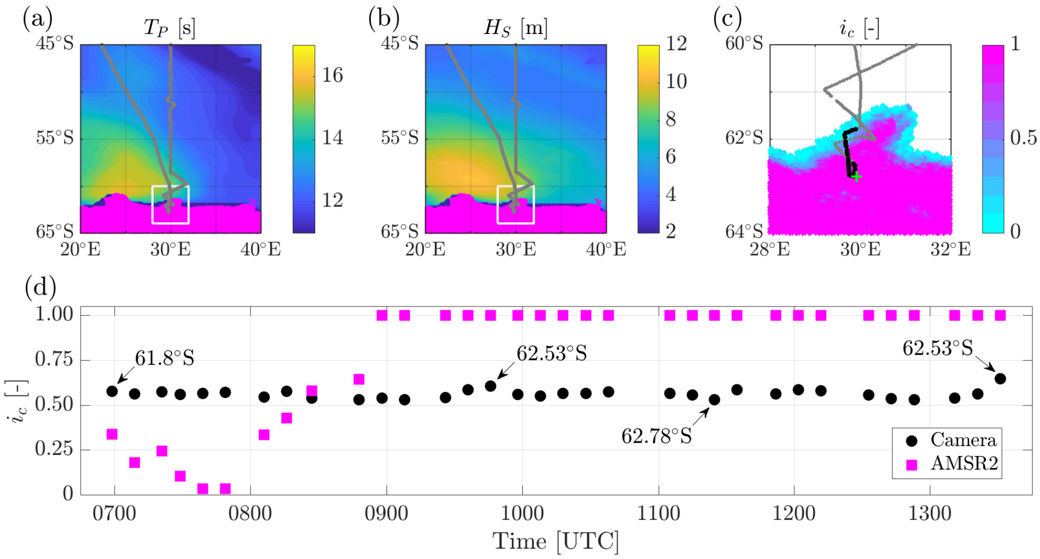

Figure 1. Environmental condition during on the 4th of July 2017 (local time UTC+2). Peak wave period (a) and significant wave height (b) are sourced from ECMWF ERA-Interim reanalysis. The magenta area denotes ice and grey dots show the ship track. In (c), ice concentration is sourced from AMSR2 satellite with a 3.125 km resolution (Beitsch et al., 2014). The black dots denotes the position during which cameras were operational and the green cross the location of deployment of a wave buoy. In (d), pancake floe concentration reconstructed from the camera images is shown as black dots, and total ice concentration obtained from AMSR2 satellite at the location closest to the measurements is shown as magenta squares.

A system of two GigE monochrome industrial CMOS cameras with a 2/3 inches sensor was installed on the monkey bridge of the icebreaker to monitor the ocean surface. The cameras were equipped with 5 mm C mount lenses (maximum aperture $f/1.8$) to provide a field of view of approximately 90°. The cameras were installed at an elevation of $\approx$ 34 m from the waterline and with their axes inclined at 20° with respect to the horizon. The system was operated by a laptop computer. Images were recorded with resolution of 2448$\times$2048 pixels and a sampling rate of 2 Hz during daylight on the 4th of July (from 07:00 to 13:30 UTC).

An automatic algorithm was developed using the MatLab Image Processing Toolbox (Kong and Rosenfeld, 1996) to extract sea ice metrics from the recorded images (see Fig. 2a for an example). To ensure statistical independence of the data set, only one camera and one image every 10 s was selected for processing. Images were rectified to correct for camera distortion and to project them on a common horizontal plane. A pixel to meter conversion was applied by imposing camera-dependent calibration coefficients. The resulting field of view is 28 m$\times$28 m and resolution 29 px/m (see Fig. 2b). The image was processed to eliminate the vessel from the field of view, adjust the image contrast, and convert the grey scales into a binary map based on a user selected threshold. The mapping isolates the solid ice shapes from background water or frazil ice. The binary images, however, are noisy and require refining based on morphological image processes to improve the shape of the pancakes floes. Threshold selection and morphological operations are optimised to detect pancake floes only and exclude interstitial frazil ice.

The Cryosphere Discuss., https://doi.org/10.5194/tc-2018-155
Manuscript under review for journal The Cryosphere
Discussion started: 1 August 2018

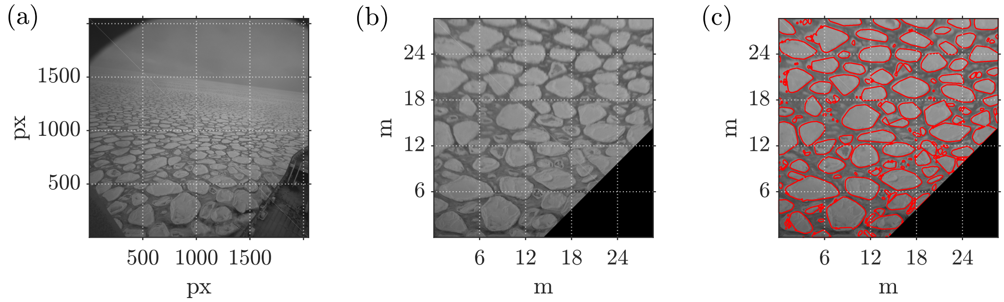

Figure 2. Sample acquired image (a), rectified and calibrated image (b) and detected pancakes (c).

The resulting separated floes are shown in Fig. 2c. Post-processed images were visually inspected for quality control, and $\approx 5\%$ of the images were discarded due to unsatisfactory reconstruction of the pancakes.

Identification of individual pancakes allows estimation of the individual floe areas A. An overall ice concentration (i_c, Fig. 1d) can be computed as the ratio of the area covered by pancake floes to the total surface in the field of view. A representative concentration was estimated every 60 consecutive images (i.e. 10 min time window), which is equivalent to a sampled area of 0.047 km^2. Pancake concentration was consistently $\approx 60\%$ with no significant variations throughout the day (Fig. 1d). The pancake concentration observed diverged from satellite observations (AMSR2) of sea ice concentration (see Fig. 1d), as the AMSR2 concentration includes the interstitial frazil ice, which is intentionally excluded from the image processing (i.e. detection of pancake ice only). Moreover, satellite data are an average over two daily swaths. Due to the intense storm activity at that time, this average may not be fully representative of the instantaneous conditions. In this regard, bridge observations following the Antarctic Sea Ice Processes and Climate protocol (ASPeCt, Worby et al., 2008), indicated a 90–100% concentration of total ice, where pancake ice was the primary ice type with concentration of 50–60% for most of the cruise (de Jong et al., 2018), in agreement with the image processing.

3 Pancake ice shape and floe size distribution

Approximating the floe shape as an ellipse, major (D_1) and a minor (D_2) axes are extracted. It is common practice, however, to define one representative dimension as a characteristic diameter $D = \sqrt{4A/\pi}$, by assuming that the pancake is a disk (Toyota et al., 2016). Only floes entirely within the field of view are considered for these operations. Detection of small floes with $D < 0.25$ m is prone to error and excluded from the analysis. Moreover, a small fraction of large floes ($< 10\%$ of floes larger than 5 m) were artificially welded by the image processing. These floes were also excluded. In total, 4×10^5 individual floes were considered over an equivalent sampled area of ≈ 1.55 km^2, and spanning almost 100 km of marginal ice zone.

Fig. 3a presents a scatter plot of the aspect ratio ($D_1 : D_2$). On average D_1 is $\approx 60\%$ greater than D_2 (slope of a linear fit). It is interesting to note that this aspect ratio is similar to the one observed for broken ice floes (Toyota et al., 2011). Fig. 3b

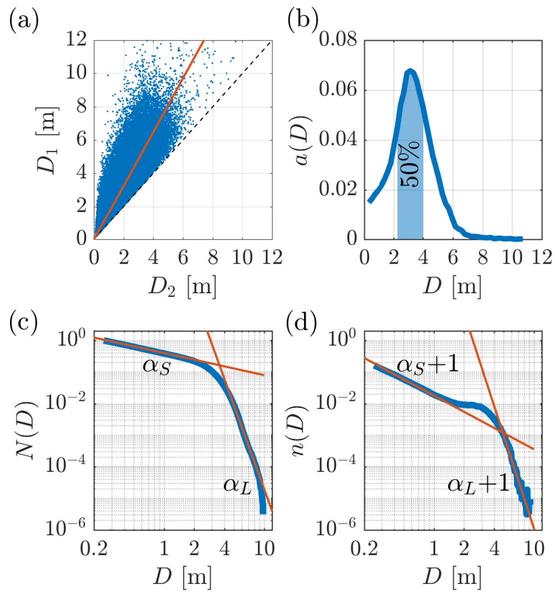

Figure 3. In (a), scatter plot of the major and minor axis of the pancake floe with the linear fit (solid orange line). In (b), ice area distribution as a function of the floe diameter. In (c), floe number exceedance probability $N(D)$ as a function of the floe diameter with two power law (solid orange lines) fitted for small ($D < 2.3$ m) and large floes ($D > 4$ m) respectively. In (d), floe number probability density function $n(D)$ as a function of the floe diameter with two power law (solid orange lines) fitted for small ($D < 2.3$ m) and large floes ($D > 4$ m) respectively.

shows that, in terms of the equivalent diameter (D), 50% of the pancake area is comprised of floes with diameters in the range 2.3–4 m. The mode of the distribution is 3.1 m, compared to $D_1 = 4$ m and $D_2 = 2.6$ m using the major and the minor axes.

Fig. 3c shows the exceedance probability $N(D)$, which exhibits two distinct slopes in the log-log plot, with a smooth transition from mild to steep slopes around the dominant diameter of 3.1 m. The probability density function of the equivalent diameter $n(D)$, shown in Fig. 3d, displays a pronounced hump in the transition between, revealing a third regime (2.3 m$< D <$ 4 m) around the modal pancake diameter, which is hidden in the exceedance probability.

Assuming, as standard, a power law $N(D) \propto D^{-\alpha}$ as a benchmark and using the maximum likelihood method, we determine $\alpha = \alpha_S = 1.1$ for small floes ($D < 2.3$ m) and $\alpha = \alpha_L = 9.4$ for large floes ($D > 4$ m). (Note that the maximum recorded diameter was $D = 10.8$ m, and, therefore, the estimation of the scaling exponent for $D > 4$ m is rigorously not applicable, as less than a decade of length scale is available.) Therefore, according to the power-law fit, the large-floe slope is ≈ 8.5 times greater than the small-floe slope. Small floes ($D < 2.3$ m) constitute the vast majority of the total detected floes ($> 80\%$). In this regime, the mild slope of $N(D)$ may result from a continuous process of floes accretion (from frazil to larger pancakes) regulated predominantly by thermodynamic freezing processes (Roach et al., 2018b). Floes larger than 4 m are detected far less frequently ($< 5\%$ of the total floes), and the steeper slope indicates that their size is governed by different underlying physical mechanisms. Visual examination of the acquired images shows that the majority of the large floes are composed of two or more

The Cryosphere Discuss., https://doi.org/10.5194/tc-2018-155
Manuscript under review for journal The Cryosphere
Discussion started: 1 August 2018

welded pancakes. The welding process is promoted by the high concentration of pancakes and the presence of interstitial frazil ice (Roach et al., 2018b).

The power-law fit is an approximation only, and an objective Kolmogorov–Smirnov goodness-of-fit test (Clauset et al., 2009) reveals that the empirical pancake size distribution does not scale accordingly to a power law in either the small- or large-floe regime, noting that the characteristic diameter itself is a crude (although often useful) metric to quantify floe size. A close inspection at the empirical distribution shows that $N(D)$ possesses a slightly concave-down curvature across all the diameter ranges (in a log-log plane) and the corresponding $n(D)$ displays a S-shape in the small-floe regime (it shifts from a concave-down to a concave-up curvature at $D \approx 1\,\mathrm{m}$) in contrast to the hypothesis of a power law behaviour. Deviations from the power law scaling are prominent towards the extremes of the intervals ($D \to 0.25\,\mathrm{m}$ and $D \to 2.3\,\mathrm{m}$ for the small-floe regime; $D \to 4\,\mathrm{m}$ and $D \to 10\,\mathrm{m}$ for the large-floe regime) but become conspicuous only by examining the empirical distribution over limited diameter ranges and probability intervals (i.e. zooming in on Figs. 3c–d).

Goodness-of-fit tests also rule out floe size distributions such as the truncated power law (Stern et al., 2018), generalized Pareto (Herman, 2010), and linear combination of Gaussian distribution and power law (Herman et al., 2017). It appears that an accurate approximation of the floe size distribution (in the goodness-of-fit sense) can only be achieved by dropping any a priori assumptions on the functional shape, e.g. by using a nonparametric kernel density estimation (Botev et al., 2010). However, this does not provide any insight on the underlying physical processes responsible for the shape of the empirical distribution.

4 Conclusions

Observations of pancake ice floe sizes during the winter expansion of the Antarctic marginal ice zone were analysed. An automatic floe detection algorithm was used to extract metrics (diameter and area) of the pancake floes, for which the equivalent diameter ($D = \sqrt{4A/\pi}$) ranged between 0.25–10 m. This allowed a quantitative representation of the pancake size distribution to be discussed.

The floe size distribution displays three distinct regimes, which are visible in the probability density function. One regime is $D = 2.3$–$4\,\mathrm{m}$, centred around the dominant pancake diameter of 3.1 m, which covers half of the total pancake area, and appears as a hump in the probability density function. Two different behaviours qualitatively close to power law scalings are observed for smaller and larger pancakes. The small-floe regime ($D < 2.3\,\mathrm{m}$), in which pancakes are experiencing thermodynamic growth, is characterised by a mild negative slope (in terms of the floe number exceedance and probability density function), while the large-floe regime, in which floes are typically formed by welding, is characterised by a much steeper slope.

Competing interests. The authors declare that they have no conflict of interest.

Acknowledgements. The cruise was funded by the South African National Antarctic Programme through the National Research Foundation. This work was motivated by the Antarctic Circumnavigation Expedition (ACE) and partially funded by the ACE Foundation and Ferring Pharmaceuticals. Support from the Australian Antarctic Science Program (project 4434) is acknowledged. MO was supported by the "Departments of Excellence 2018–2022" Grant awarded by the Italian Ministry of Education, University and Research (MIUR) (L.232/2016). CE was supported under NYUAD Center for global Sea Level Change project G1204. The authors thank Lotfi Aouf at Meteo France for providing reanalysis data and the editor Ted Maksym for useful comments. AA and AT acknowledge support from the Air-Sea-Ice Lab Project. MO acknowledges B GiuliNico for interesting discussions. AA, AT and MO thank LE Fascette for technical support during the cruise.

The Cryosphere Discuss., https://doi.org/10.5194/tc-2018-155
Manuscript under review for journal The Cryosphere
Discussion started: 1 August 2018

References

Beitsch, A., Kaleschke, L., and Kern, S.: Investigating high-resolution AMSR2 sea ice concentrations during the February 2013 fracture event in the Beaufort Sea, Remote Sensing, 6, 3841–3856, https://doi.org/10.3390/rs6053841, 2014.

Bennetts, L. G., O'Farrell, S., and Uotila, P.: Brief communication: Impacts of ocean-wave-induced breakup of Antarctic sea ice via thermodynamics in a stand-alone version of the CICE sea-ice model, The Cryosphere, 11, 1035–1040, https://doi.org/10.5194/tc-11-1035-2017, 2017.

Botev, Z. I., Grotowski, J. F., and Kroese, D. P.: Kernel density estimation via diffusion, The annals of Statistics, 38, 2916–2957, 2010.

Clauset, A., Shalizi, C., and Newman, M.: Power-Law Distributions in Empirical Data, SIAM Review, 51, 661–703, https://doi.org/10.1137/070710111, 2009.

de Jong, E., Vichi, M., Mehlmann, C. B., Eayrs, C., De Kock, W., Moldenhauer, M., and Audh, R. R.: Sea Ice conditions within the Antarctic Marginal Ice Zone in WInter 2017, onboard the SA Agulhas II, https://doi.org/10.1594/PANGAEA.885211, 2018.

Dee, D., Uppala, S., Simmons, A., Berrisford, P., Poli, P., Kobayashi, S., Andrae, U., Balmaseda, M., Balsamo, G., Bauer, P., Bechtold, P., Beljaars, A., van de Berg, L., Bidlot, J., Bormann, N., Delsol, C., Dragani, R., Fuentes, M., Geer, A., Haimberger, L., Healy, S., Hersbach, H., Hólm, E., Isaksen, L., Kållberg, P., Köhler, M., Matricardi, M., McNally, A., Monge-Sanz, B., Morcrette, J., Park, B., Peubey, C., de Rosnay, P., C., T., Thépaut, J., and Vitart, F.: The ERA–Interim reanalysis: configuration and performance of the data assimilation system, Quarterly Journal of the Royal Meteorological Society, 137, 553–597, https://doi.org/10.1002/qj.828, 2011.

Gherardi, M. and Lagomarsino, M. C.: Characterizing the size and shape of sea ice floes, Scientific reports, 5, 10 226, 2015.

Herman, A.: Sea-ice floe-size distribution in the context of spontaneous scaling emergence in stochastic systems, Phys. Rev. E, 81, 066 123, https://doi.org/10.1103/PhysRevE.81.066123, 2010.

Herman, A., Evers, K.-U., and Reimer, N.: Floe-size distributions in laboratory ice broken by waves, The Cryosphere Discussions, 2017, 1–20, https://doi.org/10.5194/tc-2017-186, 2017.

Horvat, C. and Tziperman, E.: The evolution of scaling laws in the sea ice floe size distribution, Journal of Geophysical Research: Oceans, 122, 7630–7650, https://doi.org/10.1002/2016JC012573, 2017.

Kong, T. Y. and Rosenfeld, A.: Topological algorithms for digital image processing, vol. 19, Elsevier, 1996.

Roach, L., Horvat, C., Dean, S., and Bitz, C.: An emergent Sea Ice Floe Size Distribution in a Global Coupled Ocean–Sea Ice Model, Journal of Geophysical Research: Oceans, https://doi.org/10.1029/2017JC013692, 2018a.

Roach, L., Smith, M., and Dean, S.: Quantifying Growth of Pancake Sea Ice Floes Using Images From Drifting Buoys, Journal of Geophysical Research: Oceans, https://doi.org/10.1002/2017JC013693, 2018b.

Rothrock, D. A. and Thorndike, A. S.: Measuring the sea ice floe size distribution, Journal of Geophysical Research: Oceans, 89, 6477–6486, https://doi.org/10.1029/JC089iC04p06477, 1984.

Shen, H. H. and Ackley, S. F.: A one-dimensional model for wave-induced ice-floe collisions, Annals of Glaciology, 15, 87–95, https://doi.org/10.3189/1991AoG15-1-87-95, 1991.

Shen, H. H., Ackley, S. F., and Yuan, Y.: Limiting diameter of pancake ice, Journal of Geophysical Research: Oceans, 109, https://doi.org/10.1029/2003JC002123, 2004.

Steer, A., Worby, A., and Heil, P.: Observed changes in sea-ice floe size distribution during early summer in the western Weddell Sea, Deep Sea Research Part II: Topical Studies in Oceanography, 55, 933 – 942, https://doi.org/10.1016/j.dsr2.2007.12.016, 2008.

Stern, H., Schweiger, A., Zhang, J., and Steele, M.: On reconciling disparate studies of the sea-ice floe size distribution, Elem Sci Anth, 6, https://doi.org/10.1525/elementa.304, 2018.

Toyota, T., Haas, C., and Tamura, T.: Size distribution and shape properties of relatively small sea-ice floes in the Antarctic marginal ice zone in late winter, Deep Sea Research Part II: Topical Studies in Oceanography, 58, 1182 – 1193, https://doi.org/10.1016/j.dsr2.2010.10.034, 2011.

Toyota, T., Kohout, A., and Fraser, A. D.: Formation processes of sea ice floe size distribution in the interior pack and its relationship to the marginal ice zone off East Antarctica, Deep Sea Research Part II: Topical Studies in Oceanography, 131, 28 – 40, https://doi.org/10.1016/j.dsr2.2015.10.003, 2016.

Wadhams, P., Aulicino, G., Parmiggiani, F., Persson, P. O. G., and Holt, B.: Pancake Ice Thickness Mapping in the Beaufort Sea From Wave Dispersion Observed in SAR Imagery, Journal of Geophysical Research: Oceans, https://doi.org/10.1002/2017JC013003, 2018.

Worby, A. P., Geiger, C. A., Paget, M. J., Van Woert, M. L., Ackley, S. F., and DeLiberty, T. L.: Thickness distribution of Antarctic sea ice, Journal of Geophysical Research: Oceans, 113, https://doi.org/10.1029/2007JC004254, 2008.